



LncRNA NRON promotes tumorigenesis by enhancing MDM2 activity toward tumor suppressor substrates

Qiannan Guo^{1,2,†}, Yihui Li^{1,3,†}, Yunmei Zhang^{1,4,†}, Liping Shen^{1,4}, Huayue Lin^{1,4}, Jianing Chen^{1,4}, Erwei Song^{1,4,*}  & Man-Li Luo^{1,3,**} 

Abstract

The E3 ligase MDM2 promotes tumor growth and progression by inducing ubiquitin-mediated degradation of P53 and other tumor-suppressing proteins. Here, we identified an MDM2-interacting lncRNA NRON, which promotes tumor formation by suppressing both P53-dependent and independent pathways. NRON binds to MDM2 and MDMX (MDM4) via two different stem-loops, respectively, and induces their heterogenous dimerization, thereby enhancing the E3 ligase activity of MDM2 toward its tumor-suppressing substrates, including P53, RB1, and NFAT1. NRON knockdown dramatically inhibits tumor cell growth *in vitro* and *in vivo*. More importantly, NRON overexpression promotes oncogenic transformation by inducing anchorage-independent growth *in vitro* and facilitating tumor formation in immunocompromised mice. Clinically, NRON expression is significantly associated with poor clinical outcome in breast cancer patients. Together, our data uncover a pivotal role of lncRNA that induces malignant transformation of epithelial cells by inhibiting multiple tumor suppressor proteins.

Keywords long noncoding RNA; MDM2; NRON; tumorigenesis

Subject Categories Cancer; Post-translational Modifications & Proteolysis; RNA Biology

DOI 10.15252/emboj.2022112414 | Received 21 August 2022 | Revised 15 June 2023 | Accepted 19 June 2023 | Published online 29 June 2023

The EMBO Journal (2023) 42: e112414

Introduction

Oncogenic transformation of epithelial cells is coupled with their uncontrolled proliferation and apoptosis resistance driven by multiple oncogenes. Among them, murine double minute 2 (MDM2), a

key E3 ligase, drives sustaining cell proliferation and apoptosis evasion (Vassilev, 2007). Aberrant expression of MDM2 due to its amplification or mutation is critically involved in the oncogenic transformation and uncontrolled growth of many human malignancies and correlates with poor prognosis of the cancer patients (Oliner *et al*, 2016). It is well known that MDM2 is a major regulator of P53, which forms a negative feedback loop with P53 to exert its oncogenic function (Bond *et al*, 2005; Shi & Gu, 2012). In addition, MDM2 may also induce oncogenesis via P53-independent pathways by promoting the degradation of other tumor suppressors, such as RB1 and NUMB (Fahraeus & Olivares-Illana, 2014). Importantly, the ligase activity of MDM2 depends on its dimerization with other MDM molecules, especially forming heterodimers with MDMX (MDM4; Wade *et al*, 2010). However, mechanisms underlying MDM2 heterodimerization with MDMX remain obscure.

LncRNAs act as another layer of regulators in cancer biology (Schmitt & Chang, 2016), and lncRNA dysfunction has tremendous impacts on the progression of various cancers. Not only lncRNAs provide epigenetic regulation to oncogenes and tumor suppressor genes, but ours and other studies have also shown that a major class of lncRNAs interact with signaling proteins to modulate protein–protein interaction and their activation (Schmitt & Chang, 2016; Yao *et al*, 2019). As a master tumor suppressor, P53 is associated with several lncRNAs that regulate its stability and functions (Lin *et al*, 2019). Among them, DINO lncRNA stabilizes P53 through RNA–protein interaction and regulates the P53-dependent DNA damage response (Schmitt *et al*, 2016). GUARDIN, a P53-responsive lncRNA, is critical for guarding genomic integrity and protects cells from the genotoxic stress (Hu *et al*, 2018). The P53-induced lncRNA SPARCLE is required for p53-mediated apoptosis (Meza-Sosa *et al*, 2022). Although MDM2 has been shown as a major negative regulator for P53 and contributes to tumor formation, whether lncRNAs may play a role in its enzymatic activity and oncogenic function is unknown. Here, we investigated whether lncRNAs may interact

1 Guangdong Provincial Key Laboratory of Malignant Tumor Epigenetics and Gene Regulation, Guangdong–Hong Kong Joint Laboratory for RNA Medicine, Sun Yat-Sen Memorial Hospital, Sun Yat-Sen University, Guangzhou, China
 2 Department of Thyroid Surgery, Sun Yat-Sen Memorial Hospital, Sun Yat-Sen University, Guangzhou, China
 3 Medical Research Center, Nanhai Translational Innovation Center of Precision Immunology, Sun Yat-Sen Memorial Hospital, Sun Yat-Sen University, Guangzhou, China
 4 Breast Tumor Center, Sun Yat-Sen Memorial Hospital, Sun Yat-Sen University, Guangzhou, China
 *Corresponding author. Tel: +86 20 81332603; E-mail: songew@mail.sysu.edu.cn
 **Corresponding author. Tel: +86 20 81332405; E-mail: luomli@mail.sysu.edu.cn
 †These authors contributed equally to this work

with MDM2 to regulate its ligase activities and thus play a role in oncogenesis and tumor growth.

Results

LncRNA NRON binds to MDM2 and is overexpressed in breast cancer tissues

We performed the RNA immunoprecipitation (RIP) to discover MDM2-associated lncRNAs in breast cancer cells. To identify those lncRNAs that interact with MDM2 and function in both P53-dependent and P53-independent ways, we performed RIP sequencing using the Flag antibody in MCF7 (wild-type P53) and MDA-MB-231 (mutant P53) cells overexpressing Flag-MDM2 (Fig 1A). The top abundant lncRNAs concordantly enriched in both cells were selected for validation using RIP followed by qRT-PCR. LncRNA NRON was consistently enriched in Flag-MDM2 precipitated RNA in MCF7 and MCF10A (wild-type P53), MDA-MB-231 and T47D (mutant P53) breast cancer cells (Fig 1B). In addition, we performed RIP in the breast cancer cell lines MDA-MB-436 (p53-null) and HCC1937 (p53-truncated) and found that NRON could also be enriched by Flag-MDM2 in these cells (Fig EV1A).

NRON has been reported to present in a large protein complex that contains NFAT1, IQGAP1, importin family members and kinases in T lymphocytes to regulate NFAT1 dephosphorylation and nuclear trafficking (Willingham *et al*, 2005; Sharma *et al*, 2011). Intriguingly, we observed an increased NRON expression in breast cancer cell lines. NRON level was low in normal or immortalized breast epithelial cell lines MCF10A and HMEC, but was higher in breast cancer cell lines, as detected by qRT-PCR (Fig EV1B).

To confirm the clinical significance of NRON in cancer, we compared NRON expression by *in situ* hybridization (ISH) in tissue sections of normal breast (adjacent to tumors), hyperplasia, ductal carcinoma in situ (DCIS), and invasive ductal carcinoma (IDC). NRON expression was almost undetectable or very low in normal breast tissues and began to increase in hyperplasia breast tissues and DCIS. High levels of NRON could be observed in DCIS and IDC tissues (Fig 1C and D).

We then performed ISH in a cohort of breast cancer specimens with clinicopathological information ($n = 326$; Fig 1E). NRON signals were mainly detected in the nuclei of tumor cells in the breast cancer tissues (Fig 1C). Luminal tumor tissues expressed relative lower NRON than HER2+ and triple-negative breast cancer (TNBC)

tissues (Fig 1F). In the 168 breast cancer patients with follow-up data, high NRON level was associated with higher mortality in all breast cancer patients ($P = 0.0011$). When divided into the luminal, HER2+ and TNBC subgroups, NRON also tended to be associated with poor disease-free survival (DFS) in each subgroup, especially in the TNBC subgroup which had a hazard ratio (HR) as high as 3.12. Although the association did not reach statistical significance, it might be due to the small sample size in each subgroup. Intensive NRON expression was significantly associated with larger tumor size, advanced tumor stage, and lymph node metastasis in all breast cancer tissues (Fig 1G and H). Together, these results demonstrated that NRON was an MDM2-binding lncRNA whose overexpression was of prognostic significance in breast cancer tissues.

Oncogenic roles of NRON in regulating breast cancer cell growth and apoptosis

Human NRON has been shown to be alternatively spliced to yield transcripts ranging in size from 800 to 3,700 nt. To characterize the sequence and expression of NRON in breast cancer, we performed 5' and 3' RACE and confirmed that it was a 2,730 nt transcript in MCF7 and BT474 breast cancer cells (Fig EV1C). Unlike previous report that NRON was a cytoplasmic lncRNA (Willingham *et al*, 2005), we found the majority of NRON was distributed in the nuclei of breast cancer cells, as detected by qRT-PCR after subcellular fractionation and fluorescence *in situ* hybridization (FISH; Fig EV1D and E). Coding potential prediction showed that NRON was not able to encode proteins or small peptides, as analyzed by CPPred (Tong & Liu, 2019) and prediction algorithms implemented in LNCipedia (Volders *et al*, 2019).

To silence NRON, we intended to use locked nucleic acids (LNAs) to induce RNase-H-mediated degradation due to its nuclear localization. However, eight LNAs spanning the locus failed to reduce NRON expression. We then knocked down its expression by siRNAs. Two of the siRNAs, which knocked down NRON expression about 40–50%, suppressed cell growth (Fig 2A–D) and induced G0/G1 arrest in both p53 wild-type cell MCF7 and p53 mutant cell AU565 (Fig 2E–H). Silencing NRON also increased the apoptosis induced by chemotherapeutic drugs, such as cisplatin and cyclophosphamide in MCF7 cells, as assayed by Annexin V/PI staining (Fig 2I–L). As the knockdown efficiency of NRON siRNAs was not high, we used the CRISPR approach to target NRON promoter, which decreased its expression about 70% (Appendix Fig S1A). In line with the findings of siRNA knockdown, NRON CRISPR reduced the cell proliferation, as assayed by the cell viability (Appendix

Figure 1. NRON binds to MDM2 and is overexpressed in breast cancer tissues.

- A Heatmaps of RIP sequencing showing the lncRNAs enriched in RNA precipitated by Flag-tagged MDM2. Red arrow points to NRON (ENST00000517270).
- B RIP and qRT-PCR validation of top 8 lncRNAs in four breast cell lines.
- C NRON expression in representative paraffin-embedded tissues of normal breast (adjacent tissue of breast tumors), hyperplasia breast tissues, ductal carcinoma in situ (DCIS), and invasive ductal carcinoma (IDC) tissues, as detected by ISH. ISH signals are detected as blue/purple staining with nuclei counterstained by nuclear fast red. Scale bar, 50 μ m.
- D Statistical analysis of NRON staining index in (C).
- E NRON expression in representative paraffin-embedded tissues of breast cancer tissues detected by ISH. Scale bar, 50 μ m.
- F Statistical analysis of NRON staining index in the paraffin-embedded tissues of breast cancer subtypes.
- G Kaplan–Meier survival curves of breast cancer patients with high or low NRON expression in different breast cancer subtypes.
- H The association of NRON expression with clinicopathological parameters in the paraffin-embedded tissues of breast cancer patients.

Data information: (D) and (F) are shown as mean \pm SD and analyzed with two-tailed Student's *t*-test. Source data are available online for this figure.

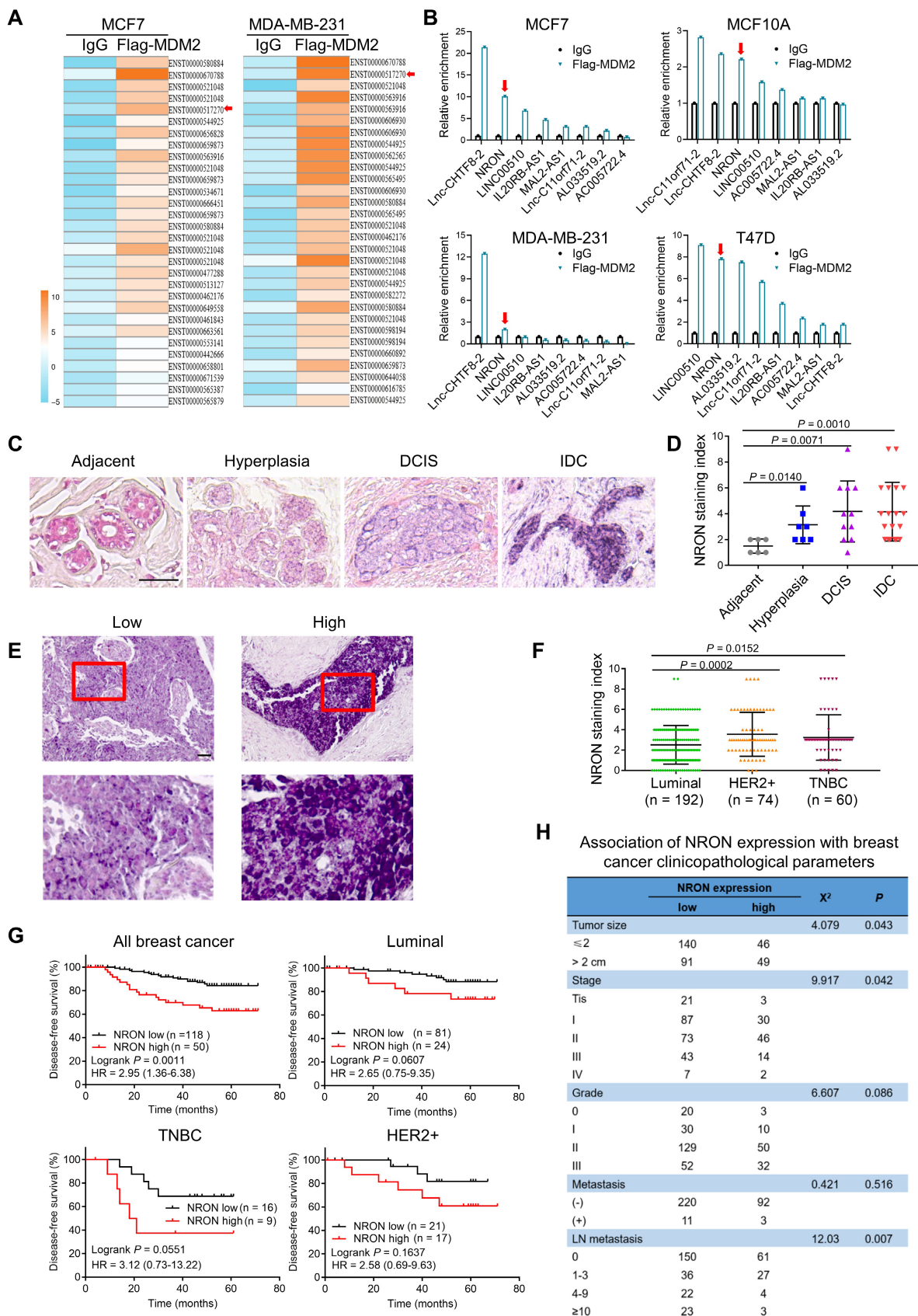


Figure 1.

Fig S1B), and induced G₀/G₁ arrest of MCF7, as assayed by flow cytometry cell cycle analysis (Appendix Fig S1C). Thus, NRON knockdown suppresses breast cancer cell growth and induces cell cycle arrest and apoptosis.

Next, we overexpressed NRON in MCF7, which expressed medium level of NRON, and in normal or immortalized breast epithelial cell lines MCF10A and HMEC which expressed low level of NRON (Fig 2M). Ectopic NRON overexpression, whose level was similar to high level of endogenous NRON in T47D and BT474 cells (Appendix Fig S1D), reduced G₀/G₁ cell percentages (Fig 2N and O) and increased cell proliferation (Fig 2P). Overexpressing NRON also protected MCF7 cells from cisplatin-induced apoptosis and decreased the sensitivity to cisplatin (Appendix Fig S1E–H). Colony formation assay showed that enforced NRON expression dramatically enhanced the capability of MCF10A and HMEC cells in forming colonies in plates and in the soft agar (Fig 2Q and R).

NRON specifically interacts with MDM2 and MDMX

To gain insight into the mechanism of NRON function, we performed RNA pulldown using *in vitro* biotin-labeled NRON and its antisense RNA to capture binding proteins. The prey complex was separated by SDS–PAGE, and differential bands captured by NRON and antisense RNA were cut for the mass spectrometry analysis (Fig 3A). Intriguingly, among the proteins identified by mass spectrometry, MDM2 and MDMX were the top two proteins bound to NRON, but not to the antisense RNA (Figs 3B and EV2A). We further validated these interactions by RNA pulldown combined with western blot using MDM2 and MDMX antibodies. Notably, in untreated cells, we could only detect the interaction of NRON with MDM2 and MDMX, but not with documented MDM2 substrates (Yoeli-Lerner *et al*, 2005; Fahraeus & Olivares-Illana, 2014), such as P53, NFAT1, and NUMB, whereas RNA pulldown in MCF7 cells treated with the proteasome inhibitor MG132, which inhibited the degradation of substrates, displayed binding of NRON to MDM2 substrates P53, NFAT1, and NUMB (Fig 3C), indicating that these substrates were in a complex with NRON before degradation.

Using MDM2 and MDMX antibodies, we performed RIP followed by qRT–PCR and confirmed the interaction of NRON with these two proteins in MCF7 cells (Fig 3D and E). We also performed RIP using P53 and NFAT1 antibodies under MG132 treated or untreated conditions and found that NRON was not enriched in P53 and NFAT1

immunoprecipitated RNAs (Fig EV2B). Even in MG132 treated cells, although NRON enrichment increased in NFAT1 immunoprecipitated RNAs, the increased fold was much less than that in MDM2 and MDMX immunoprecipitates (Fig EV2B). These results suggested that NRON bound to MDM2 and MDMX, but not through MDM2 substrates. By FISH and immunostaining, we detected a colocalization of NRON with MDM2 in MCF7 cells, mostly in the nuclear (Fig EV2C). We further detected the RNA–protein interaction using RNA electrophoretic mobility shift assay (EMSA). *In vitro*-transcribed Cy5-labeled NRON bound to both MDM2 and MDMX in the assay (Figs 3F and G, and EV2D). As the protein concentration increased, NRON bound to more recombinant MDM2 and MDMX *in vitro* (Fig 3H–K).

To map the region in NRON that bound to MDM2 and MDMX, we constructed a series of truncated mutants of NRON for the RNA pulldown assay (Fig 3L and M). The mutants containing nucleotides 1,261–1,530 of NRON exhibited the same binding capability with MDM2 as the full-length NRON, whereas other mutants lacking this region failed to bind MDM2 (Fig 3L). RNA structure softwares Mfold (Zuker, 2003) and RNAfold (Denman, 1993) independently predicted two stem-loops within 1,261–1,530 nt in NRON (Fig 3N). To test whether NRON interacts with MDM2 and MDMX through these stem-loops, we synthesized biotinylated fragments of stem-loop 1 and stem-loop 2. Consistent with the deletion experiment, RNA pulldown with synthesized fragments exhibited that stem-loop 1 and stem-loop 2 bound to MDM2 and MDMX, respectively (Fig 3O).

Next, we identified NRON-binding domains on MDM2 and MDMX using Flag-tagged fragments of MDM2 and HA-tagged fragments of MDMX. MDM2 fragments lacking the Zn-finger and RING domain (Δ 276–491) failed to bind to biotinylated NRON. Similarly, MDMX fragments containing Zn-finger and RING domain (aa 290–490) bound to NRON (Fig 3P and Q). MDM2 has been shown to interact with ribosomal RNA and p53 mRNA both through the RING domain (Elenbaas *et al*, 1996; Candeias *et al*, 2008), suggesting that the C-terminal RING domain has the RNA-binding capacity. It is very likely that NRON also interacts with the RING domain of MDM2 and MDMX.

NRON interacts with MDM2 and MDMX to promote the degradation of MDM2 substrates

We then sought to dissect the functional consequence of NRON interaction with MDM2 and MDMX. NRON knockdown or

Figure 2. Roles of NRON in regulating breast cancer cell growth and apoptosis.

- A–D (A, C) Knockdown efficiency of NRON siRNA in MCF7 and AU565 cells. Cells were transiently transfected with negative control siRNA (NC) or siRNA targeting NRON (siNRON-1 and siNRON-2). (B, D) NRON knockdown suppresses the cell viability, as quantitated by the ATP presence of viable cells 3 days after siRNA transfection.
- E–H NRON knockdown induces G₀/G₁ cell cycle arrest in MCF7 and AU565 cells. Cell cycle was measured by staining of propidium iodide (PI) followed by flow cytometric analysis. Statistics of cell percentage was shown in (F and H) as mean \pm SD of triplicate experiments.
- I–L NRON knockdown cells are more sensitive to apoptosis. MCF7 cells were transiently transfected with siNC, siNRON-1, and siNRON-2 and then treated by chemotherapy drugs cisplatin (10 μ M) for 24 h (I and J) or cyclophosphamide (5 μ M) for 36 h (K and L). Apoptosis was assayed by Annexin V/PI staining.
- M Ectopic NRON expression in breast cells, as detected by RT–PCR and agarose gel electrophoresis.
- N, O NRON overexpression promotes progression of G₀/G₁ phase. MCF7 and HMEC cells stably transfected with NRON or control vector were detected by cell cycle assay.
- P NRON overexpression promotes the proliferation of immortalized human mammary epithelial cells MCF10A and HMEC.
- Q, R Effects of NRON overexpression in promoting foci formation and colony formation in soft agar. Bar graphs were mean \pm SD, $n = 3$.

Data information: Data represent mean \pm SD from three independent experiments. *P*-values were calculated by two-tailed Student's *t*-test, as compared to the negative control groups (siNC or vector).

Source data are available online for this figure.

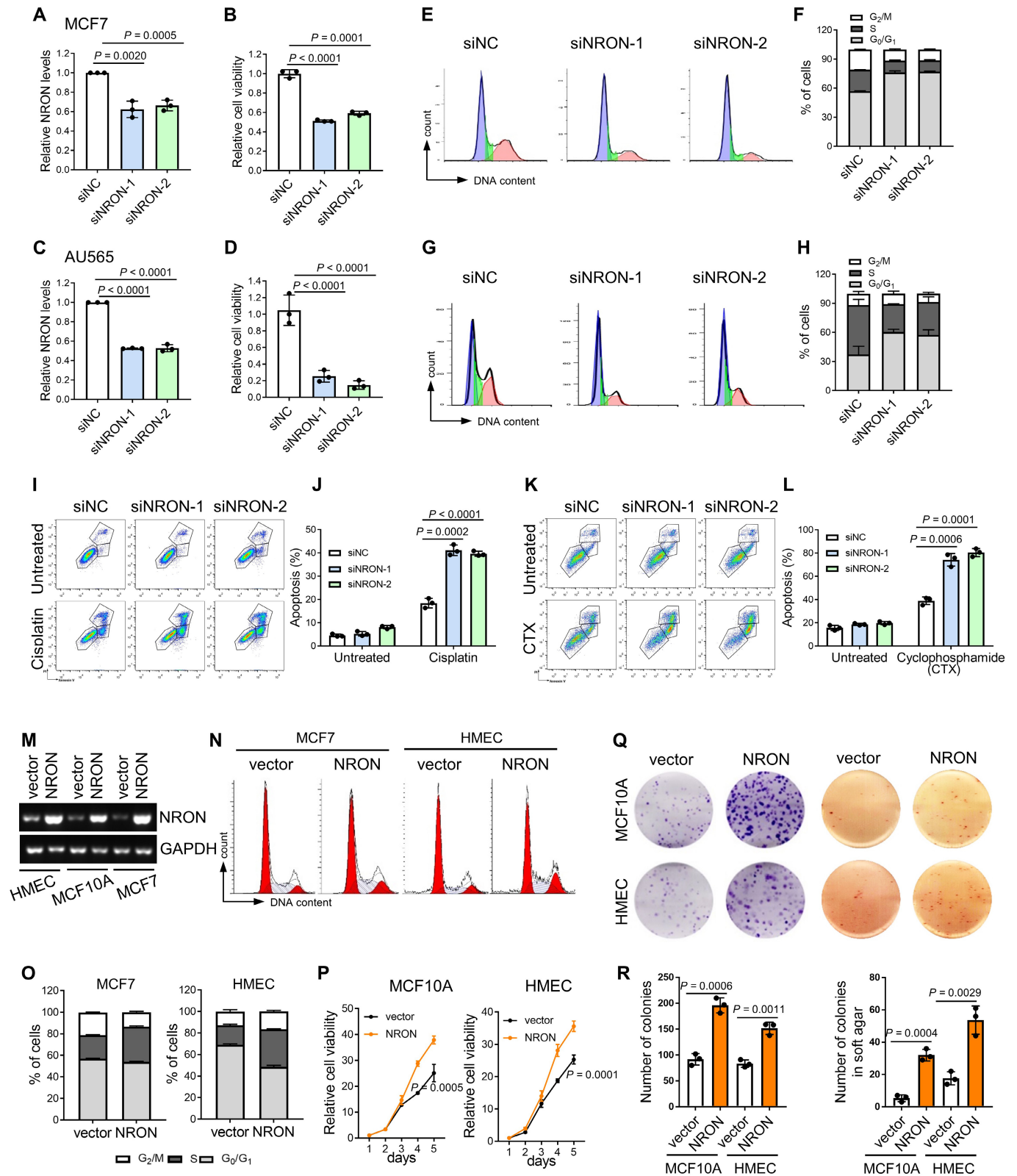


Figure 2.

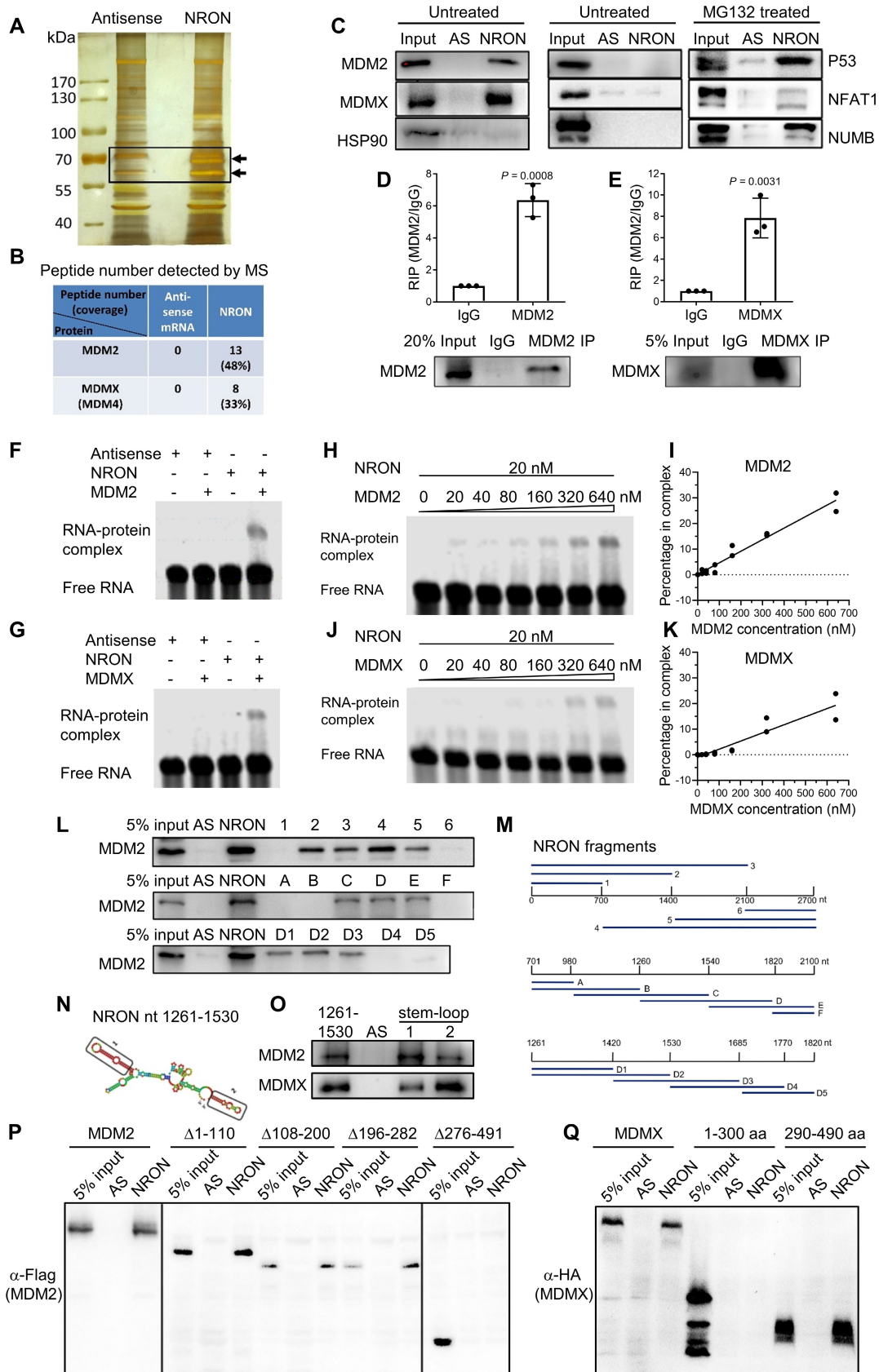


Figure 3.

Figure 3. NRON specifically interacts with MDM2 and MDMX.

- A, B Identification of NRON-interacting proteins by RNA pull-down followed by mass spectrometry in MCF7. Specific protein bands bound to NRON, but not the negative control (antisense) RNA on the SDS-PAGE gel were identified by mass spectrometry, and the number of detected peptides for candidate proteins was shown in (B).
- C RNA pull-down of NRON with MDM2 and MDMX in MCF7 cells. RNA pull-down was performed using NRON or its antisense RNA (AS), followed by western blot detection. Before protein extraction, cells were treated with or without 20 μ M MG132 for 4 h to inhibit the degradation of MDM2 substrates.
- D, E RNA immunoprecipitation (RIP) of MDM2 and MDMX in MCF7 cells. NRON was retrieved by MDM2 and MDMX IP, compared with IgG, as detected by qRT-PCR in MCF7 cells.
- F, G RNA EMSA showing binding of *in vitro*-transcribed NRON with MDM2 and MDMX. Antisense RNA was used as a negative control.
- H–K RNA EMSA showing binding of NRON with increasing concentrations of recombinant MDM2 and MDMX. The RNA and protein binding ability (I and K) was shown as the ratio of the fluorescence intensity of the RNA–protein complex to the total fluorescence intensity of the unbound RNA plus the RNA–protein complex.
- L–O RNA pull-down assay determines the stem-loops in NRON interacting with MDM2 and MDMX. NRON fragments in (M) or synthesized stem-loops in (O) were used to pull-down MDM2 and MDMX, as detected by western blot in MCF7 cells. (N) Prediction of the secondary structure of NRON nt1261–1530 demonstrating stem-loop 1 and 2.
- P NRON interacts with the Zn-finger and RING domains of MDM2. MCF7 cells were transfected with Flag-MDM2 full length, Δ 1–110 (del-N-terminal domain), Δ 108–200 (del-NLS/NES), Δ 196–282 (del-Acid Domain) or Δ 276–491 (del-Zn-finger and RING domain). RNA pull-down assay was performed using NRON or AS RNA, followed by western blot detection using Flag antibody.
- Q NRON interacts with the Zn-finger and RING domains of MDMX. MCF7 cells were transfected with HA-MDMX full length, aa 1–300 (del-Zn-finger+RING domain) or aa 290–490 (Zn-finger+RING domain). RNA pull-down assay was performed using NRON or AS RNA, followed by western blot detection using HA antibody.
- Data information: (D) and (E) represent mean \pm SD from three independent experiments. *P*-values were calculated by two-tailed Student's *t*-test, as compared to the IgG groups.
Source data are available online for this figure.

overexpression did not affect the protein levels of MDM2 or MDMX (Figs 4A–I and EV2E and F). However, silencing NRON increased the protein level of P53 and other MDM2 substrates, including NFAT1, RB1, NUMB, and RPS7 in MCF7 (Figs 4B and F, EV2E and F). Moreover, silencing NRON in MDA-MB-231, the breast cancer cells with mutant P53, hardly affect P53, but also increased the level of other MDM2 substrates (Fig 4C and G). In line with the elevated P53 or RB1 levels in NRON knockdown cells, the increased mRNA level of P53 downstream genes (P21, PUMA, and BAX) was detected in MCF7 siNRON cells, and RB1-mediated transcriptional repression of downstream genes (MCM6, FOXM1, CHK1, EZH2, and DNMT1) were detected in p53 mutant MDA-MB-231 and AU565 siNRON cells (Fig EV2H). Consistently, NRON overexpression in HMEC cells downregulated the levels of all these substrate proteins (Fig 4E and I). In addition, NRON knockdown did not affect the mRNA levels of MDM2, MDMX and their substrates, such as P53, NFAT1, and RB1 (Fig EV2H).

Besides MDA-MB-231, we also detected the effect of NRON knockdown on more mutant P53 cell lines. In AU565 and Jurkat cells, NRON knockdown almost did not affect the level of mutant P53 (Figs 4D and EV2E). Literatures showed that MDM2 contribute to the degradation of mutant P53, but not as efficient as the wild-type protein (Midgley & Lane, 1997; Buschmann et al, 2000). As the

mutant P53 protein was very abundant in the three above cell lines, the effect of NRON on mutant P53 was almost undetectable (Figs 4H and EV2G).

NRON was discovered as the ncRNA repressor of NFAT1, which highly expressed in resting CD4⁺ T lymphocytes to regulate NFAT1 dephosphorylation and nuclear trafficking (Willingham et al, 2005; Sharma et al, 2011). Silencing NRON in Jurkat cells, the immortalized line of human T lymphocyte cells, also increased the protein levels of NFAT1 and other MDM2 substrates (P53, RB1, NUMB, and RPS7; Fig 4D and H). Ionomycin and PMA (phorbol 12-myristate 13-acetate) were shown to activate T cells and induce NFAT1 dephosphorylation (Sharma et al, 2011). After stimulated with ionomycin and PMA, while Jurkat cells showed activation, as assessed by CD69 level, and NFAT1 dephosphorylation, MCF7 cells could not be activated as T cells and did not show NFAT1 dephosphorylation (Appendix Fig S2A and B). However, treated or untreated MCF7 both showed increased level of NFAT1 in NRON knockdown cells (Appendix Fig S2C).

Given that the mRNA level of P53 and other MDM2 substrates was not influenced by NRON, we hypothesized that NRON might affect their protein degradation. Cycloheximide chase assay exhibited that P53 was much more stable in NRON knockdown MCF7

Figure 4. NRON enhances the degradation of MDM2 substrates.

- A NRON knockdown or overexpression efficiency in cell lines.
- B–D NRON knockdown increases the protein level of MDM2 substrates, but not MDM2 and MDMX.
- E NRON overexpression decreases the protein level of MDM2 substrates.
- F–I Quantifications of the relative protein levels in B–E. Bar graphs were mean \pm SD, *n* = 3.
- J–M Cycloheximide (CHX) chase analysis of P53 degradation in MCF7 cells. Fifty μ g/mL CHX was added to the culture medium at indicated time points before the cell lysates were harvested. P53 levels were quantified in (L) and (M).
- N, O NRON promotes P53 ubiquitination in MCF7 cells. Cells with stable knockdown or overexpression of NRON were treated with 20 μ g/mL MG132 for 4 h before harvesting. Proteins were immunoprecipitated by P53 antibody or IgG and then detected by immunoblot (IB) of Ubiquitin (Ub).
- Data information: Data represent mean \pm SD from three independent experiments. All data were normalized to the loading control ACTB or HSP90 protein levels. *P*-values were calculated by two-tailed Student's *t*-test.
Source data are available online for this figure.

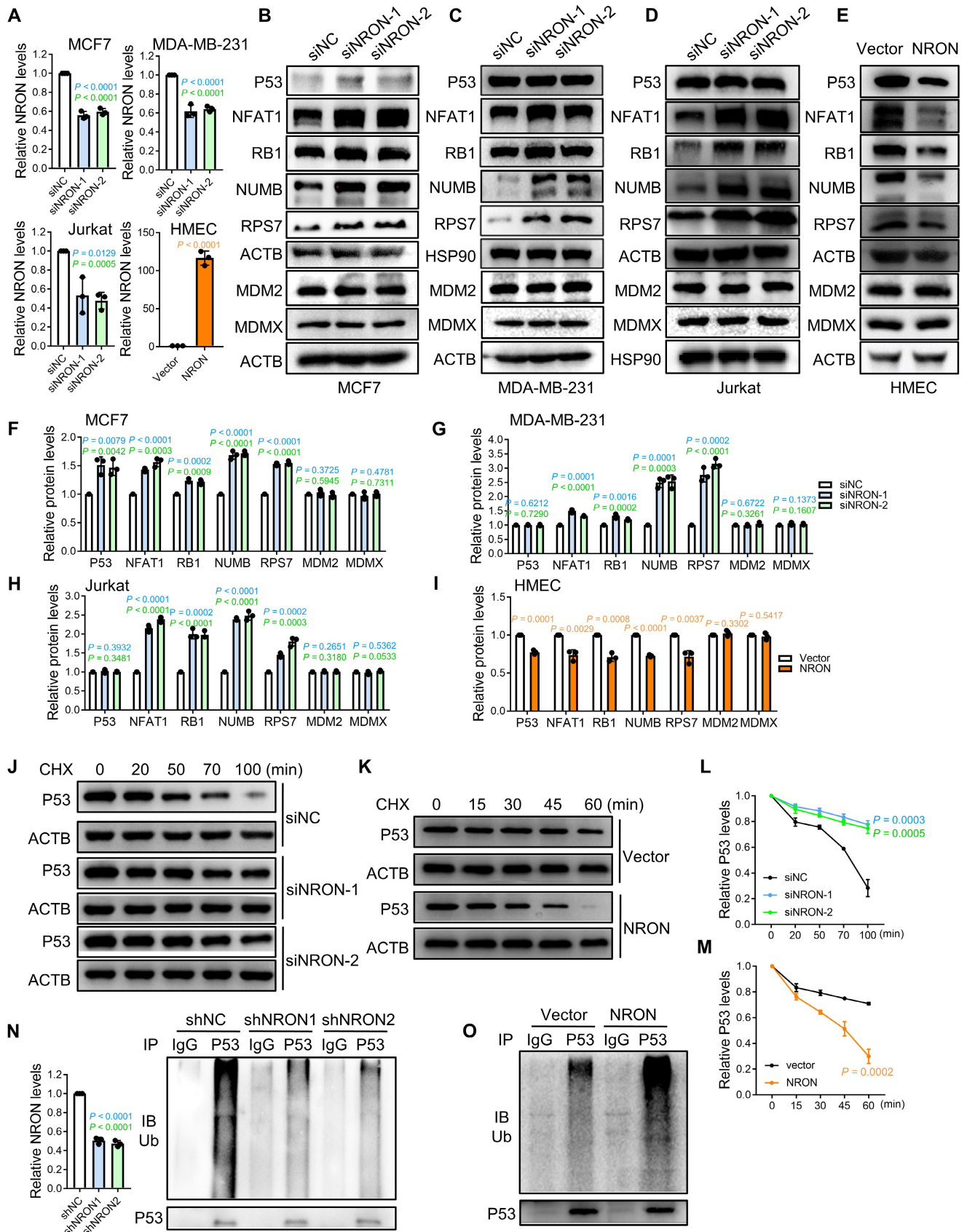


Figure 4.

cells, whereas NRON overexpression showed opposite effects (Fig 4J–M). We then treated MCF7 cells with MG132 and immunoprecipitated P53 for the detection of P53 ubiquitination using the antiubiquitin antibody. P53 was ubiquitinated less in the NRON knockdown cells and more efficiently ubiquitinated in NRON-overexpressing cells than control cells (Fig 4N and O). Parallel experiments examining NFAT1 stability revealed that NRON knockdown stabilized NFAT1 protein, while NRON overexpression had the opposite effect (Appendix Fig S2D–G). However, no difference was detected in the stability of mutant P53 between control and NRON knockdown MDA-MB-231 cells (Appendix Fig S2H and I). Thus, NRON promotes the degradation of wild-type P53 and NFAT1 in breast cancer cells.

Furthermore, we investigated the expression correlation between NRON and MDM2 substrates in primary tumor tissues. Given that NRON did not affect the level of mutant P53, and wild-type P53 expression was relatively low in most of the tumor tissues, we thus examined the association of NRON with NFAT1 expression in breast cancer tissues. Regardless of P53 status, 35 out of 135 samples (25.9%) with high level of NRON showed weak staining of NFAT1, while 31/135 samples (23%) with low level of NRON displayed high expression of NFAT1 (Appendix Fig S2J and K). Statistical analysis showed a negative correlation between NRON and NFAT1 expression in these breast cancer tissues ($P = 0.001$, $R = -0.297$).

NRON promotes the heterodimerization of MDM2 and MDMX

The E3 ligase activity of MDM2 can be regulated by several mechanisms, including MDM2 modifications, association with protein regulators, and homo-oligomerization or hetero-oligomerization with MDMX (Wade et al, 2010; Fahraeus & Olivares-Illana, 2014). Since NRON interacted with both MDM2 and MDMX, we speculated that NRON might promote the heterodimerization of MDM2 and MDMX to enhance MDM2 activity toward substrates. Co-immunoprecipitation (Co-IP) experiments demonstrated that knockdown of NRON impaired the interaction between MDM2 and MDMX (Fig 5A), whereas NRON overexpression increased the binding of MDM2 to MDMX in MCF7 (Fig 5B).

We next used *in vitro* competition assay to examine whether NRON promoted MDM2 heteromeric complex formation instead of homodimer formation. MCF7 cells were co-transfected with low or high doses of myc-MDM2 and a constant dose of HA-MDMX (Fig 5C). With increasing amounts of MDM2 expressed, more myc-MDM2 were pulled down by GST-MDM2 in the lysate of vector control cells. However, in the lysate of NRON-overexpressing cells, GST-MDM2 still bound to HA-MDMX even when the cells expressed high level of myc-MDM2 (Fig 5C).

To directly detect MDM2 and MDMX dimer formation, we used cross-linking reagent glutaraldehyde to treat the lysates of MCF7 cells ectopically expressing Flag-MDM2 and HA-MDMX. The cross-linked dimers were resolved by electrophoresis and detected by western blots using antibodies against Flag or HA. In NRON knock-out MCF7 cells, more MDM2 homodimer was formed than in the negative control cells (Fig 5D). In NRON-overexpressing cells, more MDM2-MDMX heterodimer was formed than in the vector control MCF7 cells (Fig 5D). Reciprocal western blots detecting MDMX dimers confirmed these results (Fig 5E).

MDM2 and its substrates mediate the oncogenic effects of NRON

As NRON knockdown increased the level of P53, RB1, and other tumor suppressors in MCF7 cells, we hypothesized that these MDM2 substrates mediated the effects of NRON knockdown. Cisplatin-induced apoptosis was increased in NRON knockdown MCF7 cells, and this effect was abolished by the P53 siRNAs (Fig 6A–C), but not the NFAT1 siRNAs (Fig EV3A–C). In p53 mutant cells MDA-MB-231 and AU565, NRON knockdown did not increase the cisplatin-induced apoptosis (Fig EV3D–G). These results suggested that P53 might be the major downstream mediator of NRON in regulating apoptosis. We then examined whether P53 mediated the effect of NRON on cell proliferation. Silencing P53 increased the proliferation of MCF7 cells and partially restored the viability of NRON knockdown cell (Fig EV3H and I), indicating that the effect of NRON on cell growth only partially act through P53.

To test whether NRON acts through other MDM2 substrates in P53 mutant cells, we silenced RB1 in MDA-MB-231 and AU565 cells (Fig 6E and I). NRON knockdown reduced the colony formation and cell proliferation in MDA-MB-231 and AU565 cells, and RB1 siRNAs partially rescued this effect (Fig 6D–K). We also tested whether NFAT1 mediated the effect of NRON on the cell growth. Silencing NFAT1 increased cell growth and partially abolished the inhibitory effects of NRON knockdown on cell growth, as detected by foci formation and proliferation assay in MDA-MB-231 cells (Fig EV3J–M).

Next, we asked whether NRON mutants, which failed to interact with MDM2 or MDMX, would affect the level of MDM2 substrates. Overexpression of full-length NRON decreased the level of P53, NFAT1, RB1, and RPS7 (Fig 6L), as well as promoted cell growth and colony formation in HMEC-Ras cells (Fig 6M–Q). However, overexpression of M1 (deletion mutant of stem-loop 1), M2 (deletion mutant of stem-loop 2), and M3 (deletion mutant of stem-loop 1 and 2) failed to reduce the level of MDM2 substrates, or accelerate the cell growth (Fig 6L–Q), confirming that binding to MDM2 or MDMX was essential for NRON to exert its oncogenic function.

Notably, human NRON could interact with mouse Mdm2 and Mdmx in NIH3T3 cells (Fig EV4A). Knockdown of mouse NRON in NIH3T3 could reduce foci formation, induce cell cycle G0/G1 arrest, and increase the transcription of P53 downstream targets (Fig EV4B–G). Next, we overexpressed human NRON or three mutants in NIH3T3. We found human NRON could also reduce the level of Mdm2 substrates, as well as promote NIH3T3 proliferation and colony formation, while none of the mutants showed such effects (Fig 6L–Q).

To directly investigate whether NRON functioned through MDM2, we overexpressed NRON in MDM2 knockdown and p53/MDM2 double knockdown cells. In HMEC-Ras and NIH3T3 cells, silencing MDM2 or silencing both MDM2 and P53 using human and mouse siRNAs, respectively (Fig 6S), abrogated the effect of NRON overexpression in the soft agar colony formation (Fig 6R and T). These data suggested that MDM2 mediated the oncogenic effects of NRON.

NRON plays a tumorigenic role *in vivo*

To evaluate the effect of knocking down NRON *in vivo*, we generated the Tet-On inducible NRON knockdown cells, which targeted the same sequence as siRNA-2 of NRON (Appendix Table S1). First,

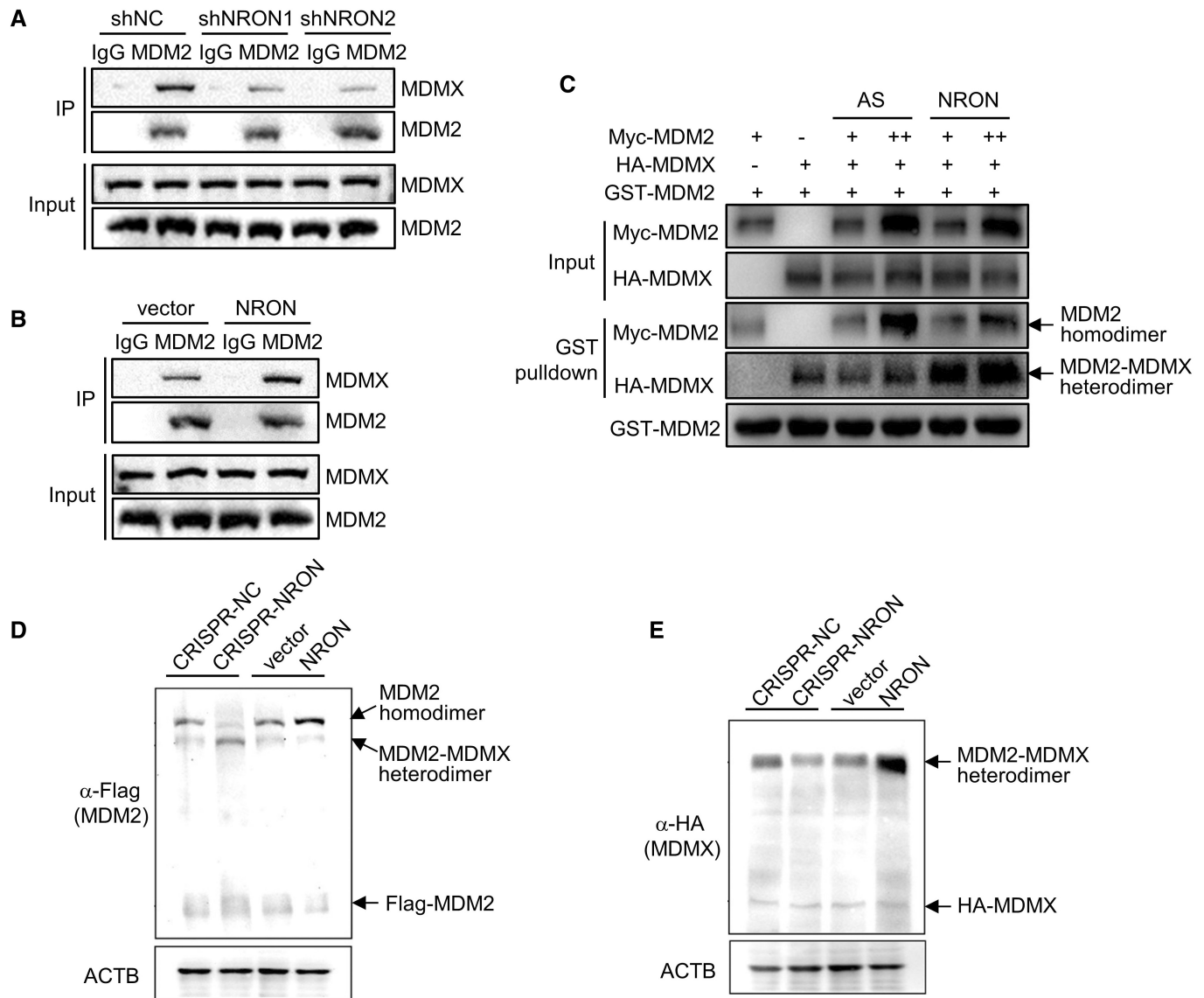


Figure 5. NRON promotes the heterodimerization of MDM2 with MDMX.

A, B NRON promotes the interaction of MDM2 and MDMX, as detected by co-immunoprecipitation in stable cell lines with NRON knockdown or overexpression. The lysates of indicated MCF7 cells were incubated with MDM2 antibody or IgG. The immunoprecipitated proteins were subjected to immunoblot with MDMX antibody.

C Competition binding assay of GST-MDM2 to MDM2 and MDMX. Lysates of MCF7 cells transfected with constant amount of HA-MDMX and increasing amount of myc-MDM2 were incubated with GST-MDM2 beads. NRON or antisense RNA was added to the incubation mixture, and the interacting proteins with GST-MDM2 were assayed by immunoblot.

D, E NRON promotes the formation of MDM2 and MDMX heterodimers. MCF7 lysates were incubated with the cross-linking reagent glutaraldehyde and subjected to immunoblot to detect Flag-tagged MDM2 (D) and HA-tagged MDMX (E).

Source data are available online for this figure.

we confirmed that the Tet-On system had similar knockdown efficiency and phenotypes as the siRNA by detecting the cell proliferation and colony formation in MCF7 cells (Fig EV5A–D). Then, we used the Tet-On shRNA for animal experiments. 2×10^6 MCF7 cells expressing Tet-On shNC or shNRON were injected orthotopically into the mammary fat pads into nude mice. Growth of MCF7 xenografts was significantly suppressed upon doxycycline-induced

knockdown of NRON, as measured by the volumes and weights of xenografts (Fig 7A and B). *In vivo* knockdown efficiency of NRON was confirmed by ISH in xenograft sections (Fig 7C and E). Consistent with *in vitro* observations, silencing NRON *in vivo* decreased cell proliferation, as detected by Ki67 staining, promoted cell apoptosis, as detected by TUNEL assay, and increased the level of MDM2 substrates RB1 and NFAT1 (Fig 7C–E). Moreover, we

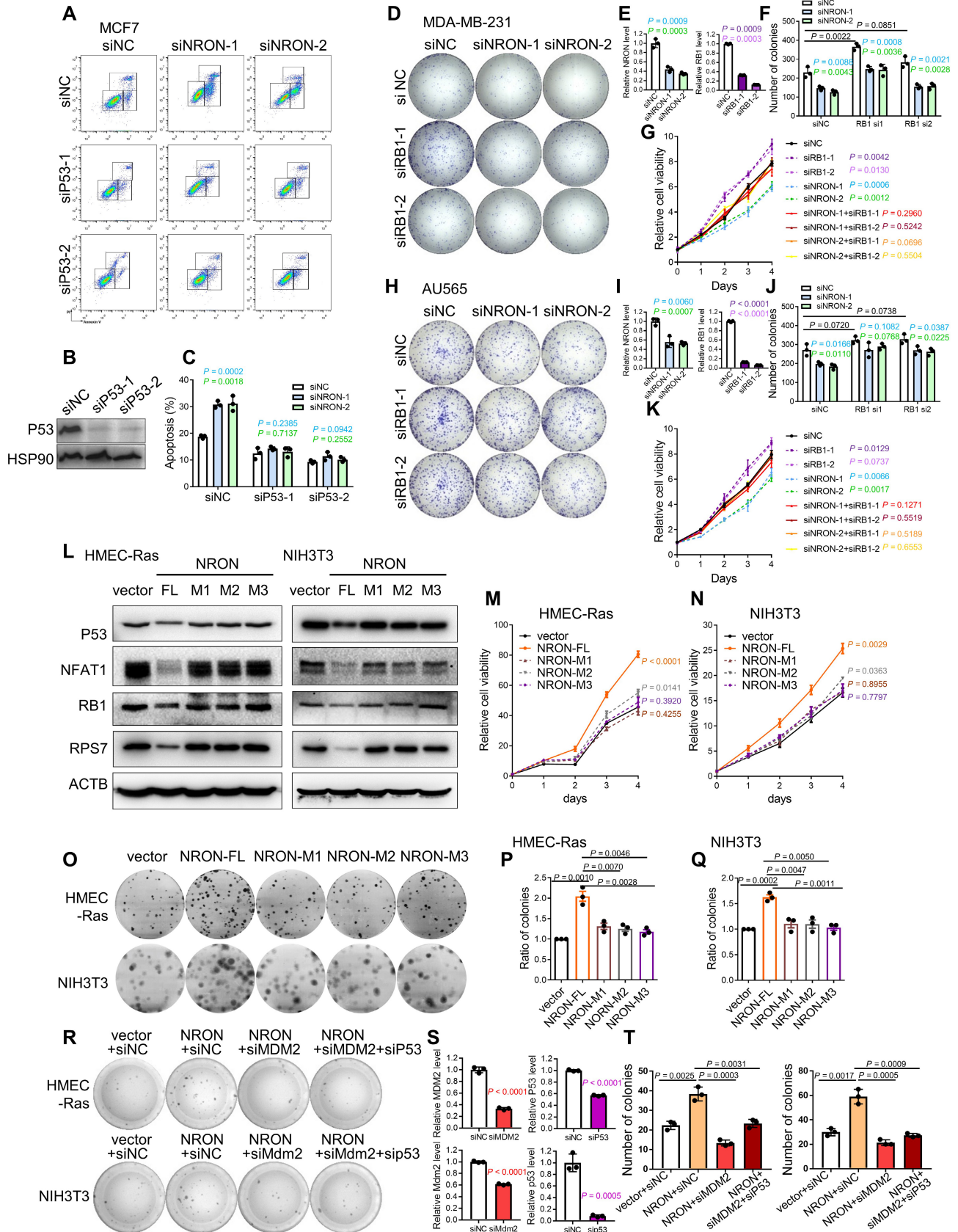


Figure 6.

Figure 6. NRON exerts its oncogenic function through promoting the degradation of MDM2 substrates.

- A–C P53 siRNAs abolish cisplatin-induced apoptosis enhanced by NRON knockdown in MCF7 cells.
 D–F RB1 knockdown partially abolishes the effect of NRON siRNAs on colony formation in MDA-MB-231 cells.
 G RB1 knockdown partially abolishes the effect of NRON siRNAs on the proliferation of MDA-MB-231 cells.
 H–J RB1 knockdown partially abolishes the effect of NRON siRNAs on colony formation in AU565 cells.
 K RB1 knockdown partially abolishes the effect of NRON siRNAs on the proliferation of AU565 cells.
 L Effects of overexpressing NRON and its mutants on regulating the level of MDM2 substrates. HMEC-Ras and NIH3T3 cells were stably transfected with indicated constructs. M1 and M2 are NRON mutants with mutation in stem-loop 1 and 2, respectively. M3 is the mutant with both mutations in stem-loop 1 and 2.
 M, N Effects of overexpressing NRON and its mutants on regulating the proliferation of HMEC-Ras and NIH3T3 cells.
 O–Q Effects of overexpressing NRON and its mutants on regulating the colony formation of HMEC-Ras and NIH3T3 cells.
 R–T Silencing MDM2 or MDM2 and P53 together abrogates the effect of NRON overexpression on regulating the colony formation of HMEC-Ras and NIH3T3 cells.

Data information: Data represent mean \pm SD from three independent experiments. *P*-values were calculated by two-tailed Student's *t*-test, as compared to the negative control groups (siNC or vector).

Source data are available online for this figure.

evaluate the xenograft growth of silencing NRON in P53 mutant MDA-MB-231 and AU565 cells. Doxycycline-induced knockdown of NRON suppressed the tumor growth of both MDA-MB-231 and AU565 xenografts (Fig EV5H–O).

To expand our findings to other cancer types, we used the lung cancer A549 cells and cervical cancer Hela cells for xenograft experiments. We confirmed that silencing NRON with Tet-on inducible system increased the protein level of MDM2 substrates in these two cell lines (Fig EV5E–G). Then, we injected the cells subcutaneously into nude mice and found that NRON knockdown reduced the growth of A549 and Hela xenografts (Fig 7F–I).

We then used HMEC cells transformed with V12H-Ras (HMEC-Ras) and NIH3T3 to test the effect of NRON overexpression on tumorigenesis. Consistent with previous literatures (Elenbaas *et al*, 2001; Mani *et al*, 2008), no tumors arose when 5×10^6 HMEC-Ras or NIH3T3 cells infected with empty vector were injected into NOD/SCID mice (Appendix Fig S3A–F). Remarkably, tumors developed in five of nine mice with NRON-overexpressing HMEC-Ras cells and four of eight mice with NRON-overexpressing NIH3T3 cells, respectively (Appendix Fig S3A–G). Then, we also evaluated the *in vivo* impact of NRON overexpression in MCF7. 1×10^6 NRON-overexpressing MCF7 cells formed tumors in five out of seven nude mice, whereas same number of vector cells formed tumors in four out of seven nude mice with smaller tumor sizes (Appendix Fig S3H–K).

Next, we queried whether overexpression of NRON mutants that failed to interact with MDM2 and MDMX induced tumor formation *in vivo*. Although six of seven nude mice inoculated with 5×10^6 full-length NRON-expressing HMEC-Ras cells formed tumors, 4, 4, 5

out of 7 mice injected with an equal number of M1, M2, and M3 cells, respectively, developed tumors with much smaller sizes (Fig 7J and K). As the vector cells did not form tumors, we could only examine NRON expression in full-length and mutant NRON-expressing xenografts. More proliferating cells, and fewer intensive NFAT1 and RB1 staining, were detected in full-length xenografts compared with mutant xenografts (Fig 7N and O). However, very few apoptotic cells were detected in full-length and mutant NRON-expressing xenografts (Appendix Fig S3L and M). In NIH3T3 xenografts, similar results were observed which showed reduced tumor incidence and smaller final tumor weights of mutant xenografts compared with full-length xenografts (Fig 7L and M). Together, these data suggest that NRON plays a critical role in tumorigenesis.

Discussion

In this paper, we uncovered the novel role of NRON in tumorigenesis where NRON enhances ubiquitin-dependent degradation of multiple tumor suppressors and promotes tumorigenesis by regulating MDM2/MDMX heterodimerization (Fig 8). NRON was first discovered as the repressor of NFAT, which was highly expressed in resting CD4⁺ T lymphocytes and regulated the dephosphorylation and nuclear trafficking of NFAT (Willingham *et al*, 2005; Sharma *et al*, 2011). NRON expression in CD4⁺ T cells could also modulate HIV transcription and replication (Li *et al*, 2016). Recently, NRON has been found expressed in a broad spectrum of tissues and cells, including bone tissues, cardiomyocytes, and vascular smooth muscle cells, and exerts diverse functions by interacting with different

Figure 7. NRON plays a tumorigenic role in the xenograft mouse model.

- A–E (A, B) NRON knockdown suppresses the growth of MCF7 xenografts in nude mice. 2×10^6 MCF7 cells stably expressing Tet-on control or NRON shRNA were injected as xenografts in nude mice. Doxycycline (200 μ g/ml) was supplied in drinking water to induce Tet-on shRNA expression. (C, E) ISH of NRON and IHC analysis in MCF7 xenografts. Representative images (C) of NRON ISH and IHC of Ki67 and MDM2 substrates RB1 and NFAT1 in paraffin-embedded sections of xenografts. Scale bar, 50 μ m. Statistical results of positive staining were shown in (E). (D, E) TUNEL assay showing apoptotic cells in MCF7 xenografts. Scale bar, 50 μ m. Statistical results of positive staining were shown in (E).
 F–I NRON knockdown suppresses the growth of A549 and Hela xenografts in nude mice. 2×10^6 cancer cells stably expressing Tet-on control or NRON shRNA were injected as xenografts in nude mice.
 J–M Effects of overexpressing NRON and its mutants on regulating tumor formation of HMEC-Ras and NIH3T3 cells. 5×10^6 indicated cells were injected in nude mice.
 N, O Representative IHC images of paraffin-embedded sections of NRON and its mutants overexpressing HMEC-Ras xenografts. Scale bar, 50 μ m. Statistical results of positive staining were shown in (O).

Data information: Data represent mean \pm SD. Replicates are $n = 7$ (A, B, F–K), $n = 8$ (L, M) or $n = 3$ (E, O). *P*-values were calculated by two-tailed Student's *t*-test.

Source data are available online for this figure.

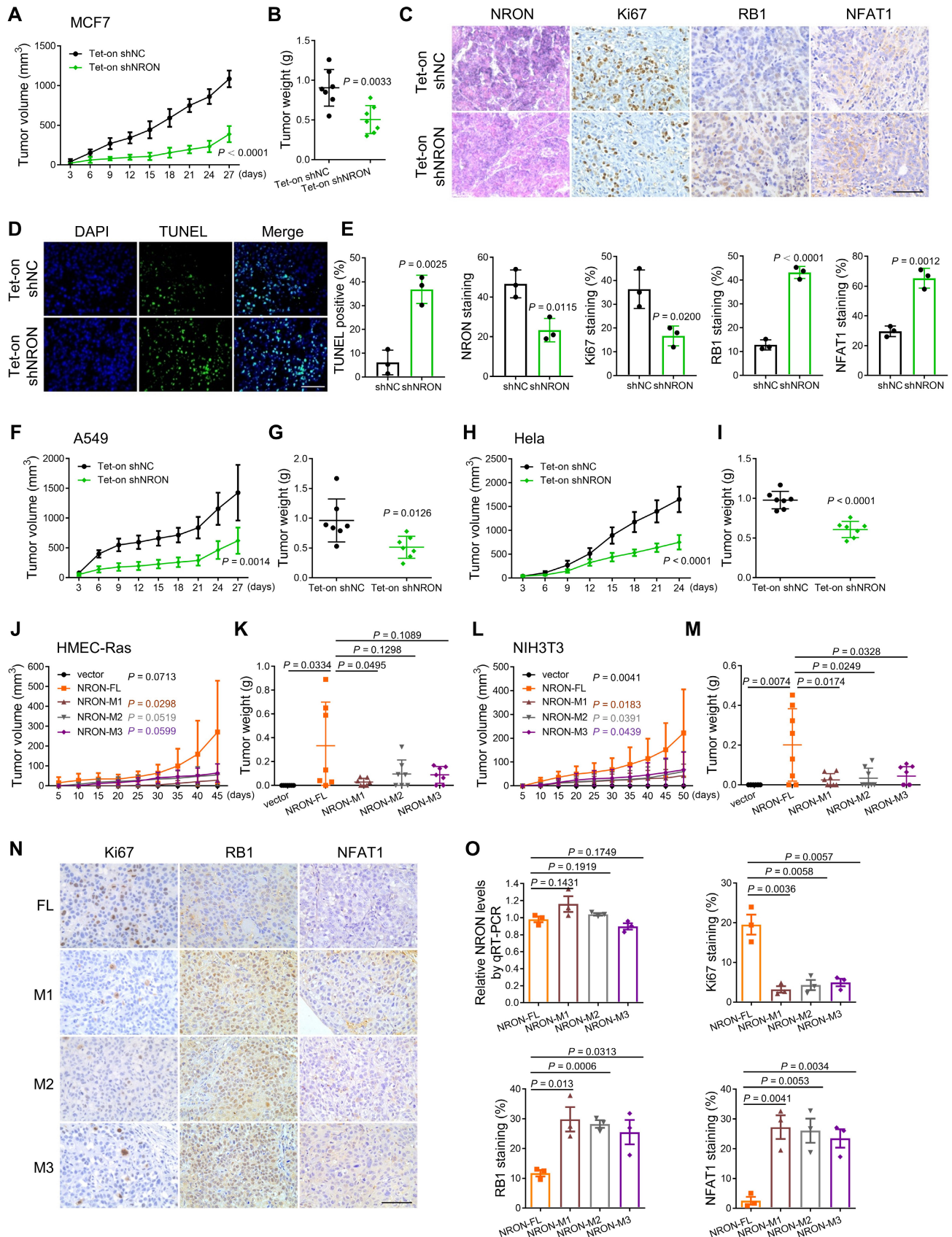


Figure 7.

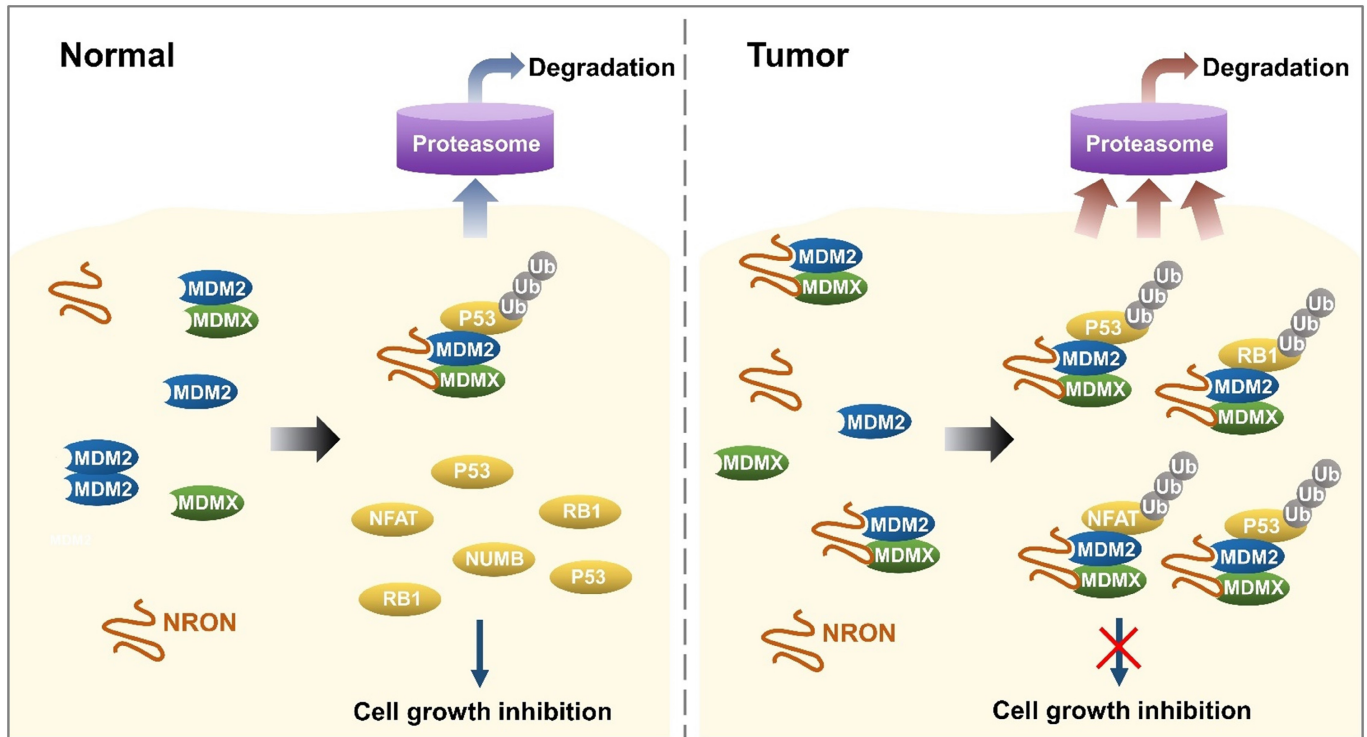


Figure 8. Schematic diagram of the role of NRON in tumorigenesis.

NRON enhances Ubiquitin-dependent degradation of multiple tumor suppressors and promotes tumorigenesis by regulating MDM2/MDMX heterodimerization.

protein partners (Jin *et al.*, 2021; Du *et al.*, 2022; Hoepfner *et al.*, 2022). Unlike in T cells, we found NRON predominantly localized in the nucleus in breast cancer cells, similar to that in the cardiomyocytes (Hoepfner *et al.*, 2022). Moreover, in breast cancer cells, NRON regulates the degradation of NFAT, but not the dephosphorylation. Interestingly, we found in Jurkat T cells, NRON can regulate both NFAT dephosphorylation and degradation. As NRON is a long lncRNA with multiple motifs, different functional motifs may interact with selective proteins in various cellular contexts. Indeed, we revealed that nucleotides 1,261–1,530 of NRON exhibited the same binding capability with MDM2 and MDMX as the full-length NRON. Similarly, nucleotides 3,037–3,391 of mouse NRON were as efficient as full-length NRON in preventing bone resorption of osteoclasts (Jin *et al.*, 2021). Thus, an attractive hypothesis is that NRON localizes in specific subcellular compartments to preferentially recruit protein complex by certain motifs and serve distinct functions in a cell context-dependent manner.

Most of the transforming oncogenes are protein-coding genes, whose overexpression converts the immortalized cell to a malignant phenotype. Here, we showed that overexpression of the lncRNA NRON induced anchorage-independent growth of immortalized cells in soft agar and tumor formation of NIH3T3 cells in immunodeficient mice. These results pointed to a potent transforming property of NRON, which could be attributed to its ability to increase the degradation of multiple tumor suppressors, including P53, RB1, and NFAT1. Besides MDM2, the well-documented oncogenes that negatively regulate multiple tumor suppressors are mostly E3 ligase, such as SKP2 which targets P21 and P27 for degradation

(Cai *et al.*, 2020), and kinases, such as AKT1 which inhibits FOXO, GSK3, and TSC2 proteins (Manning & Cantley, 2007). Our data provide the first demonstration of a lncRNA that induces malignant transformation through negatively regulating multiple tumor suppressor proteins.

There are controversial studies about the role of NRON in cancer. NRON was reported to be downregulated in triple-negative breast cancer and hepatocellular carcinoma (Yao *et al.*, 2018; Niu *et al.*, 2019). One key difference with our study is that these results were based on RT-qPCR of the whole tumor tissues, which include bulk of nontumor cells. We performed RNA ISH to detect NRON expression, which showed that NRON specifically highly expressed in breast cancer cells. NRON was also reported to inhibit breast cancer development (Mao *et al.*, 2020). In this study, NRON overexpression suppressed breast cancer cell growth. However, the sequence of NRON is inconsistent in different databases. In UCSC Genome Browser, human NRON is a 370 nt lncRNA (ENST00000517270.1 from GENCODE V41). In NCBI Gene, human NRON is a 2,730 nt lncRNA (Gene ID: 641373, NR_045006.1). According to our RACE results, which showed that NRON was 2,730 nt in both MCF7 (p53 wild-type cell) and BT474 (p53 mutant cell), we overexpressed the 2,730 nt NRON and found that it promoted breast cancer cell growth *in vitro* and *in vivo*. There are also studies supported our observations that NRON increased tumor cell growth, such as in bladder cancer and gastric Cancer (Xiong *et al.*, 2020; Wang *et al.*, 2021), as well as NRON was highly expressed in esophageal squamous cell carcinomas and inhibited cisplatin-induced cell apoptosis (Liu *et al.*, 2022).

A key mechanistic finding of our study is that NRON promotes the heterodimerization of MDM2 with MDMX, thereby increasing the E3 ligase activity of MDM2. It has long been known that MDM2 can form homodimer or heterodimer. The molecular ratio of MDM2 and MDMX to P53 appears to be a determinant for the dimerization, as the heterodimer is more effective in inducing P53 degradation, whereas the homodimer increases MDM2 autoubiquitylation (Wade *et al*, 2010). Whether there are determinants other than the stoichiometric balance remains unclear. The complete understanding of the composition of MDM2-MDMX heterocomplex is also lacking. We reveal that NRON preferentially promotes MDM2-MDMX dimerization and boosts MDM2 ligase activity for the degradation of P53 and other substrates. Intriguingly, NRON has been reported to induce the degradation of Tat to participate in HIV-1 infection. Although NRON is shown to link Tat to the ubiquitin/proteasome components including CUL4B and PSMD11 (Li *et al*, 2016), Tat protein is also a MDM2 substrate (Bres *et al*, 2003). Other mechanism, which involves MDM2, may also exist to promote Tat degradation by NRON. Our study not only demonstrates the existence of a lncRNA in the MDM2-MDMX complex but also elucidates the determinant role of NRON in regulating MDM2 heterodimerization and E3 ligase activity.

By now, MDM2 inhibitors and dual inhibitor of MDM2 and MDMX that perturb the interaction of MDM2/MDMX with wild-type P53 are vigorously being developed for cancer treatment. Efforts have also been made to target mutant P53, which occurs in about half of all tumors (Bykov *et al*, 2018). Recent data have demonstrated that dual MDM2/MDMX inhibitor exhibits marked P53 reactivation with less hematopoietic toxicity in preclinical studies and early clinical trials of solid tumors and hematologic malignancies (Chang *et al*, 2013; Carvajal *et al*, 2018; Saleh *et al*, 2021), suggesting that inhibiting MDM2 and MDMX together may achieve better therapeutic efficacy. The role of NRON in regulating MDM2/MDMX heterocomplex may have important implications for targeting MDM2/MDMX to restore wild-type P53 for cancer treatment. More than that, NRON plays an oncogenic role in P53-dependent and independent manners, which offers a unique advantage of inhibiting both P53 wild-type and mutant tumors. Thus, our study provides mechanistic insight which warrants further testing of targeting NRON in breast and other cancers with wild-type or mutant P53.

In summary, we demonstrate that NRON is a potent oncogenic lncRNA that enhances MDM2/MDMX heterodimerization and degradation of multiple tumor suppressor proteins. Our study may have the clinical implication that tumors without MDM2 amplification or overexpression may still show reduced P53 activity if NRON is overexpressed, which highlights the necessity of examining NRON level together with MDM2/MDMX and P53 status when selecting patients that will benefit from MDM2/MDMX inhibitor treatment.

Materials and Methods

Cell culture, transfection, and transduction

Cancer cell lines were obtained from American Type Culture Collection and grown according to standard protocols. For transfection of siRNA or overexpression plasmids, 2×10^5 cells were plated in 6-well plates and transfected with Lipofectamine 2000 (Invitrogen)

according to the manufacturer's instructions. For infection of lentivirus-delivered shRNAs or Tet-on shRNAs, 0.5×10^5 cells were plated in 24-well plates and transduced with lentiviral particles with 5 μ g/ml polybrene. Following the infection, cells were selected using puromycin (1 μ g/ml) to generate stable cell lines. Doxycycline (100 ng/ml) was used to induce Tet-on shRNA expression in cells.

Plasmids, oligos, and probes

For overexpression, the sequence of NRON was first identified by 5' and 3' rapid amplification of cDNA ends (RACE) and subcloned into the pcDNA3.1 vector. Then, the transfected cells were selected with G418. The shRNAs were cloned into LV3 (H1/Puro) lentiviral vector (GenePharma) or psi-LVMInU6TP (inducible U6) lentiviral vector (GeneCopoeia) for knockdown experiments. To obtain clustered regularly interspaced short palindromic repeats (CRISPR)/CRISPR-associated protein-9 (Cas9) mediated knockout of NRON, we designed guide RNAs to target the promoter sequence, but not the exons, because partial deletion of lncRNA sequence sometimes cannot abrogate its function. Two guide RNAs that generate double nicking in the NRON promoter were cloned into Lenti-sgRNA-EGFP, which was co-transfected with Lenti-cas9-puro plasmid into HEK 293FT cells to generate lentiviral particles (Hryhorowicz *et al*, 2017). The target sequences of siRNAs, shRNAs, and sgRNAs are listed in Appendix Table S1.

Cell viability, apoptosis, and cell cycle assays

For the cell viability assay, cells were seeded in 96-well plates and 12 h after seeding was defined as day 0. After 0, 1, 2, 3, and 4 days of seeding, cells were harvested and cell viability was examined by the celltiter glo kit (Promega, Fitchburg, WI) according to the manufacturer's instructions.

To induce apoptosis, cells were treated with cyclophosphamide (5 μ M) for 36 h or cisplatin (10 μ M) for 24 h and were dissociated using 0.25% trypsin-EDTA, and then collected by centrifugation. Apoptosis was determined using an Annexin V Apoptosis Detection kit purchased from eBioscience and immediately analyzed by flow cytometry (Accuri C6, BD). To study the effect of NRON expression on cell cycle, cells were harvested and stained with PI for 30 min using the Cell Cycle Detection Kit (BD Biosciences) according to the manufacturer's instructions and analyzed by flow cytometry.

Colony formation and soft agar assays

For colony formation assay, cells (500–2,000 cells/well) were plated in a 6-well plate. After culturing for 7–10 days, cells were fixed with methanol and stained with crystal violet solution. Colonies with > 50 cells per colony were counted. For soft agar assays, a bottom layer of 0.6% agar noble in DMEM without serum was first placed onto 6-cm dishes. Cells were seeded in 0.3% top agar containing complete medium. Fresh top agar was added after 1.5 week, and colonies were counted after 3 weeks.

Western blotting

Protein was extracted from the cells using RIPA buffer, resolved by SDS-polyacrylamide gels, and then transferred to polyvinylidene

difluoride membranes. Primary antibodies against p53 (CST, 2527, 1:1,000), NFAT1 (CST, 5861, 1:1,000), NUMB (CST, 2756, 1:1,000), MDM2 (Abcam, 1:1,000, ab3110), MDMX (MERCCK, 04-1555, 1:1,000), RB1 (CST, 9309, 1:100), RPS7 (NOVUS, H00006201-M03, 1:1,000) anti-Flag (Sigma, F1804, 1:1,000), anti-myc (Abcam, ab32072, 1:1,000), anti-GST (MBL, M071-3, 1:1,000), anti-HA (CST, 3724 1:1,000), ubiquitin (CST, 3936, 1:500), actin (CST, 3700, 1:1,000), and HSP90 (CST, 4877, 1:500) were used. Peroxidase-conjugated secondary antibody (CST) was used, and the antigen-antibody reaction was visualized by enhanced chemiluminescence assay (ECL, Thermo). Blots were quantified with ImageJ software.

To detect MDM2 homodimers and MDM2-MDMX heterodimers, cell lysates were incubated with 0.05% glutaraldehyde for 30 min at 4°C. The chemical cross-linking reaction was stopped by adding loading sample buffer, and the samples were boiled and analyzed by western blotting.

Northern blotting and qRT-PCR

Total RNA was subjected to northern blot assays according to the protocol provided by Roche (DIG Application Manual for filter hybridization, Roche). Detection of probe-target hybrids was performed using a DIG Luminescent Detection kit for Nucleic Acids (Roche, 11363514910), as described before (Yu *et al.*, 2007). QRT-PCR was performed using a SYBR Premix Ex Taq kit (Takara) according to the manufacturer's instructions. The northern blot probe and primers for PCR are listed in Appendix Tables S1 and S2. Data were collected and analyzed using a LightCycler 480 instrument (Roche).

Fluorescent in situ hybridization (FISH) and immunofluorescence

Cells were rinsed in PBS and fixed in 4% formaldehyde in PBS (pH 7.4) for 15 min at room temperature. Then, the cells were permeabilized in PBS containing 0.5% Triton X-100 and 5 mM vanadyl ribonucleoside complex (R3380, Sigma, St. Louis, MO) on ice for 10 min, washed with PBS 3 × 10 min, and rinsed once in 2 × SSC prior to hybridization. Using an anti-NRON oligodeoxynucleotide probe which was conjugated with Alexa Fluor 488 (Invitrogen, Carlsbad, CA) or DIG, hybridization was performed in hybridization solution (probe dilution 1:1,250; Boster, China) for 16 h at 50°C in a moist chamber. For FISH, cells were washed for 30 min in 25% deionized formamide /2 × SSC at 50°C and then at 50°C, 30 min in 2 × SSC, as described before (Chen *et al.*, 2011). For confocal microscopy, the cells on coverslips were counterstained with DAPI and imaged using a confocal laser-scanning microscope (Carl Zeiss, Oberkochen, Germany) with a core data acquisition system (Applied Precision, Issaquah, WA).

For colocalization of lncRNA and protein, cells were first hybridized with NRON probe conjugated with Alexa Fluor 488 (Invitrogen, Carlsbad, CA). Then, cells were rinsed briefly in PBS, fixed in 2% formaldehyde for 5 min, and incubated with MDM2 antibody (Abcam, ab3110, 1:1,000) at 4°C overnight. Images were obtained with a confocal laser-scanning microscope (Carl Zeiss, Oberkochen, Germany) with a core data acquisition system (Applied Precision Issaquah, WA). ImageJ software (NIH, Bethesda, MD) was used to analyze the colocalization of NRON and MDM2.

Patient tumor samples and in situ hybridization

Chemotherapy-naive invasive breast cancer samples were obtained from 326 patients with chemotherapy-naive patients from Sun Yat-sen Memorial Hospital between 2008 and 2012. All samples were collected from patients with informed consent, and all related procedures were performed with the approval of the internal review and ethics boards of Sun Yat-sen Memorial Hospital. The Approval Number was 2016-181, which was renewed as SYSKY-2023-297-01. Paraffin-embedded sections were used for *in situ* hybridization (ISH). Briefly, after dewaxing and rehydration, the samples were digested with proteinase K, fixed in 4% paraformaldehyde, hybridized with the 5'digoxin-labeled LNATM-modified NRON probe (Exiqon, Vedbaek, Denmark) at 55°C overnight, and subsequently incubated overnight at 4°C with antidigoxin monoclonal antibody (Roche, Basel, Switzerland). Then, the sections were stained with nitro blue tetrazolium/5-bromo-4-chloro-3-indolylphosphate, mounted and examined. Positive expression of NRON (in blue) was primarily detected in the nucleus. The staining scores were determined based on both the intensity and proportion of NRON-positive cells in 10 random fields under a 40× objective. The proportion of positively stained tumor cells in sections was graded as follows: 0, no positive cells; 1, < 10%; 2, 10–50%; and 3, > 50%. The cells at each staining intensity were recorded on a scale of 0 (no staining), 1 (light blue), 2 (blue), and 3 (dark blue). The staining index (SI) was calculated as follows: SI = staining intensity × proportion of positively stained cells, as described before (Liu *et al.*, 2015). Using this method, the expression of NRON was evaluated using SI and scored as 0, 1, 2, 3, 4, 6, or 9. A SI score of 3 was used as a cutoff value based on the distribution of frequency of SI score for NRON expression and a measurement of heterogeneity with the log-rank test statistic with respect to overall survival, and the expression levels of NRON were defined as high (SI > 3) or low (SI ≤ 3).

Immunohistochemistry

Paraffin-embedded slides were deparaffinized with xylene and dehydrated with graded alcohols. Antigen retrieval was performed by incubation of the slides in a pressure cooker for 5 min in 0.01 M citrate buffer, pH 6.0, and subsequent treatment with 3% hydrogen peroxide for 5 min. Then, immunohistochemistry was performed using mouse anti-Ki-67 Nuclear Antigen Monoclonal Antibody (ZSGB-BIO, China), p53 (CST, 2527, 1:100), Rb1 (CST, 9309, 1:100), and NFAT1 (CST, 5861, 1:100). Immunohistochemical staining was performed according to the Manufacturer's instructions. The accuracy of automated measurements was confirmed through independent evaluation by two pathologists. Cells stained with the indicated antibodies were counted at 630× magnification in at least 10 fields per section. To evaluate the stainings, positive cells in the blue channel were counted in four different fields using ImageJ.

Immunoprecipitation (IP) and co-immunoprecipitation (Co-IP)

Cells were lysed in IP lysis buffer and protease inhibitors. For immunoprecipitation, antibody against MDM2 (Abcam, ab3110, 1:1,000), MDMX (MERCCK, 04-1555, 1:1,000), p53 (CST, 2524, 1:1,000), and NFAT1 (CST, 5861, 1:1,000) was added to the lysates and incubated overnight at 4°C, with rabbit or mouse IgG (1–5 μg) as the control

antibody. Then, Dynabeads Protein A/G (10002D/10003D, Invitrogen) was added and then incubated for 1 h at room temperature. The retrieved proteins were then detected by western blotting.

RNA immunoprecipitation (RIP)

Cells were lysed with RIP lysis buffer supplemented with protease-inhibitor cocktail and RNase inhibitor (1,000 U/ml, Ambion) and then incubated with antibody-coated microbeads at 4°C overnight. Antibodies specific to Flag (F1804, sigma, 1:1,000), human MDM2 (Abcam, ab3110, 1:1,000), MDMX (MERCK, 04-1555, 1:1,000), p53 (CST, 2524, 1:1,000), NFAT1 (CST, 5861, 1:1,000) and control rabbit/mouse IgG (CST, 2729/5415, 1:1,000) were added to the lysates. After the immunoprecipitation, the coprecipitated RNA was extracted for RNA sequencing or qRT-PCR analysis. The RIP sequencing data were deposited in GEO database with the accession number GSE226511.

RNA pulldown

Biotin-labeled RNAs were transcribed *in vitro* with Bio-16-UTP using the MEGAscript T7 High Yield Transcription kit (Invitrogen). RNA structure buffer (10 mM Tris [pH 7.0], 0.1 M KCl, 10 mM MgCl₂) was added to 1 µg of biotinylated RNA, heated to 95°C for 2 min, put on ice for 3 min, and then left at room temperature for 30 min. Folded RNA was mixed with cell lysates or recombinant protein in 500 µl RIP buffer and then incubated at room temperature for 1 h. A total of 50 µl of washed Dynabeads M-280 Streptavidin (60210, Invitrogen) were added to each binding reaction and further incubated at room temperature for another 1 h. Beads were washed briefly with RIP buffer for five times and boiled in SDS loading buffer. The retrieved proteins were then detected by western blotting or mass spectrum analysis. Different bands pulled by NRON and antisense RNA were detected by Silver Stain Kit (P0017S, Pierce) and cut for mass spectrometry analysis (MALDI-TOF, Bruker Daltonics, Billerica MA).

RNA EMSA

RNA was labeled with cy5 by incorporating cy5-UTP into RNA while *in vitro* transcription. The cy5-labeled RNA was denatured at 60°C for 10 min and immediately placed on ice. RNA and MDM2 protein were diluted with 5× binding buffer (50 mM Tris, 250 mM KCl, 25 mM MgCl₂, 10% glycerol, 5 mM DTT and RNase inhibitor, pH 7.9), respectively. After incubated at room temperature for 10 min, diluted RNA and MDM2 protein were mixed and incubated at room temperature for 30 min. Free RNA and RNA–protein complexes were separated using 0.5% agarose gel (Daneshvar *et al.*, 2020). Images were acquired and analyzed through LI-COR Odyssey imaging system.

In vitro competitive binding assay

Myc-MDM2 and HA-MDMX constructs were transfected into breast cancer cells. The cells were lysed in IP lysis buffer. Recombinant human GST-MDM2 Protein (R&D systems, E3-202) and Glutathione Agarose were incubated at 4°C for 1 h. Then, the cell lysates were added to the beads and incubated at 4°C for 1 h with folded NRON or antisense (AS) mRNA. Binding capacity was detected by immunoprecipitation and western blotting.

In vivo mouse experiments

Mice studies were carried out according to the ethical regulations approved by Sun Yat-sen University Animal Care and Use Committee. The Approval Number was SYSU-IACUC-2020-B0276, which was renewed as AP20220107. Five-week-old female Balb/c nude mice or NOD/SCID mice were purchased from Vital River Laboratories and raised under standard conditions at the specific-pathogen-free (SPF) animal facility in the Laboratory Animal Resource Center of Sun Yat-sen University. 2×10^6 MCF-7/ AU565 or 1×10^6 MDA-MB-231 cells were injected orthotopically into the mammary fat pads of mice. 2×10^6 A549/Hela or 5×10^6 HMEC-Ras/NIH3T3 cells were injected subcutaneously over the flanks of mice in 0.1 ml of sterile PBS. To induce Tet-on shRNA expression, mice were fed with doxycycline (200 µg/ml) supplemented with 5% sucrose via drinking water, which was exchanged every 3 days. Tumor volume was calculated every 3 days according to the formula $V \text{ (mm}^3\text{)} = 0.5 \times (\text{length} \times \text{width}^2)$. Xenografts were harvested, weighed, and snap-frozen for RNA or protein extraction or fixed in formaldehyde for paraffin-embedded sections.

Statistics

Statistical analyses were performed using Prism 9.0 (GraphPad) and SPSS Statistics 20.0 (SPSS). The *P*-values were calculated with independent sample *t*-tests to compare two groups of samples, and with Mann-Whitney tests to compare the quantification of ISH and IHC data. Spearman analysis was used to measure the correlation of different variables. Survival curves were plotted with the Kaplan-Meier method and analyzed with log-rank tests. All statistical analyses were performed using two-tailed *P*-values.

Data availability

Source data and materials are available from the corresponding authors at reasonable request. All other data are contained in the main manuscript, Expanded View and Appendix Figures and Tables. The RIP sequencing data were deposited in GEO database with the accession number GSE226511 (<https://www.ncbi.nlm.nih.gov/geo/query/acc.cgi?acc=GSE226511>).

Expanded View for this article is available [online](#).

Acknowledgments

This work was supported by grants from National Key Research and Development Program of China (2021YFA1300602), National Science Foundation of China (82003276, 82002934, 82073048, 92159303, 81930081), Guangdong Science and Technology Department (2020B1212060018, 2020B1212030004), Department of Natural Resources of Guangdong Province (GDNRC[2021]51), Bureau of Science and Technology of Guangzhou (20212200003), the Program for Guangdong Introducing Innovative and Entrepreneurial Teams (2019BT02Y198).

Author contributions

Qiannan Guo: Data curation; formal analysis; validation; investigation; methodology; writing – original draft. **Yihui Li:** Data curation; formal analysis; validation; investigation. **Yunmei Zhang:** Data curation; formal analysis;

validation; investigation; writing – review and editing. **Liping Shen:** Investigation. **Huayue Lin:** Investigation. **Jianing Chen:** Resources; validation. **Erwei Song:** Conceptualization; funding acquisition; project administration; writing – review and editing. **Man-Li Luo:** Conceptualization; data curation; formal analysis; supervision; funding acquisition; writing – original draft; project administration; writing – review and editing.

Disclosure and competing interests statement

The authors declare that they have no conflict of interest.

References

- Bond GL, Hu W, Levine AJ (2005) MDM2 is a central node in the p53 pathway: 12 years and counting. *Curr Cancer Drug Targets* 5: 3–8
- Bres V, Kiernan RE, Linares LK, Chable-Bessia C, Plechakova O, Treand C, Emiliani S, Peloponese JM, Jeang KT, Coux O et al (2003) A non-proteolytic role for ubiquitin in tat-mediated transactivation of the HIV-1 promoter. *Nat Cell Biol* 5: 754–761
- Buschmann T, Minamoto T, Wagle N, Fuchs SY, Adler V, Mai M, Ronai Z (2000) Analysis of JNK, Mdm2 and p14(ARF) contribution to the regulation of mutant p53 stability. *J Mol Biol* 295: 1009–1021
- Bykov VJN, Eriksson SE, Bianchi J, Wiman KG (2018) Targeting mutant p53 for efficient cancer therapy. *Nat Rev Cancer* 18: 89–102
- Cai Z, Moten A, Peng D, Hsu CC, Pan BS, Manne R, Li HY, Lin HK (2020) The Skp2 pathway: a critical target for cancer therapy. *Semin Cancer Biol* 67: 16–33
- Candeias MM, Malbert-Colas L, Powell DJ, Daskalogianni C, Maslon MM, Naski N, Bourougaa K, Calvo F, Fahraeus R (2008) P53 mRNA controls p53 activity by managing Mdm2 functions. *Nat Cell Biol* 10: 1098–1105
- Carvajal LA, Neriah DB, Senecal A, Benard L, Thiruthuvanathan V, Yatsenko T, Narayanagari SR, Wheat JC, Todorova TI, Mitchell K et al (2018) Dual inhibition of MDMX and MDM2 as a therapeutic strategy in leukemia. *Sci Transl Med* 10: eaao3003
- Chang YS, Graves B, Guerlavais V, Tovar C, Packman K, To KH, Olson KA, Kesavan K, Gangurde P, Mukherjee A et al (2013) Stapled alpha-helical peptide drug development: a potent dual inhibitor of MDM2 and MDMX for p53-dependent cancer therapy. *Proc Natl Acad Sci USA* 110: E3445–E3454
- Chen J, Yao Y, Gong C, Yu F, Su S, Chen J, Liu B, Deng H, Wang F, Lin L et al (2011) CCL18 from tumor-associated macrophages promotes breast cancer metastasis via PITPNM3. *Cancer Cell* 19: 541–555
- Daneshvar K, Ardehali MB, Klein IA, Hsieh FK, Kratkiewicz AJ, Mahpour A, Cancelliere SOL, Zhou C, Cook BM, Li W et al (2020) lncRNA DIGIT and BRD3 protein form phase-separated condensates to regulate endoderm differentiation. *Nat Cell Biol* 22: 1211–1222
- Denman RB (1993) Using RNAfold to predict the activity of small catalytic RNAs. *Biotechniques* 15: 1090–1095
- Du M, Wang C, Yang L, Liu B, Zheng Z, Yang L, Zhang F, Peng J, Huang D, Huang K (2022) The role of long noncoding RNA Nron in atherosclerosis development and plaque stability. *iScience* 25: 103978
- Elenbaas B, Dobbelstein M, Roth J, Shenk T, Levine AJ (1996) The MDM2 oncoprotein binds specifically to RNA through its RING finger domain. *Mol Med* 2: 439–451
- Elenbaas B, Spirio L, Koerner F, Fleming MD, Zimonjic DB, Donaher JL, Popescu NC, Hahn WC, Weinberg RA (2001) Human breast cancer cells generated by oncogenic transformation of primary mammary epithelial cells. *Genes Dev* 15: 50–65
- Fahraeus R, Olivares-Illana V (2014) MDM2's social network. *Oncogene* 33: 4365–4376
- Hoepfner J, Leonardy J, Lu D, Schmidt K, Hunkler HJ, Biss S, Foinquinos A, Xiao K, Regalla K, Ramanujam D et al (2022) The long non-coding RNA NRON promotes the development of cardiac hypertrophy in the murine heart. *Mol Ther* 30: 1265–1274
- Hryhorowicz M, Lipinski D, Zeyland J, Slomski R (2017) CRISPR/Cas9 immune system as a tool for genome engineering. *Arch Immunol Ther Exp* 65: 233–240
- Hu WL, Jin L, Xu A, Wang YF, Thorne RF, Zhang XD, Wu M (2018) GUARDIN is a p53-responsive long non-coding RNA that is essential for genomic stability. *Nat Cell Biol* 20: 492–502
- Jin F, Li J, Zhang YB, Liu X, Cai M, Liu M, Li M, Ma C, Yue R, Zhu Y et al (2021) A functional motif of long noncoding RNA Nron against osteoporosis. *Nat Commun* 12: 3319
- Li J, Chen C, Ma X, Geng G, Liu B, Zhang Y, Zhang S, Zhong F, Liu C, Yin Y et al (2016) Long noncoding RNA NRON contributes to HIV-1 latency by specifically inducing tat protein degradation. *Nat Commun* 7: 11730
- Lin T, Hou PF, Meng S, Chen F, Jiang T, Li ML, Shi ML, Liu JJ, Zheng JN, Bai J (2019) Emerging roles of p53 related lncRNAs in cancer progression: a systematic review. *Int J Biol Sci* 15: 1287–1298
- Liu B, Li X, Xie J, Feng Z, Lin N, Yu M (2022) lncRNA NRON negatively regulates cisplatin-induced cell apoptosis via downregulating miR-31 in esophageal squamous cell carcinomas. *In Vitro Cell Dev Biol Anim* 58: 37–43
- Liu B, Sun L, Liu Q, Gong C, Yao Y, Lv X, Lin L, Yao H, Su F, Li D et al (2015) A cytoplasmic NF-kappaB interacting long noncoding RNA blocks IkappaB phosphorylation and suppresses breast cancer metastasis. *Cancer Cell* 27: 370–381
- Mani SA, Guo W, Liao MJ, Eaton EN, Ayyanan A, Zhou AY, Brooks M, Reinhard F, Zhang CC, Shipitsin M et al (2008) The epithelial-mesenchymal transition generates cells with properties of stem cells. *Cell* 133: 704–715
- Manning BD, Cantley LC (2007) AKT/PKB signaling: navigating downstream. *Cell* 129: 1261–1274
- Mao Q, Li L, Zhang C, Sun Y, Liu S, Li Y, Shen Y, Liu Z (2020) Long non coding RNA NRON inhibited breast cancer development through regulating miR-302b/SRSF2 axis. *Am J Transl Res* 12: 4683–4692
- Meza-Sosa KF, Miao R, Navarro F, Zhang Z, Zhang Y, Hu JJ, Hartford CCR, Li XL, Pedraza-Alva G, Perez-Martinez L et al (2022) SPARCLE, a p53-induced lncRNA, controls apoptosis after genotoxic stress by promoting PARP-1 cleavage. *Mol Cell* 82: 785–802.e10
- Midgley CA, Lane DP (1997) p53 protein stability in tumour cells is not determined by mutation but is dependent on Mdm2 binding. *Oncogene* 15: 1179–1189
- Niu L, Fan Q, Yan M, Wang L (2019) lncRNA NRON down-regulates lncRNA snaR and inhibits cancer cell proliferation in TNBC. *Biosci Rep* 39: BSR20190468
- Oliner JD, Saiki AY, Caenepeel S (2016) The role of MDM2 amplification and overexpression in tumorigenesis. *Cold Spring Harb Perspect Med* 6: a026336
- Saleh MN, Patel MR, Bauer TM, Goel S, Falchook GS, Shapiro GI, Chung KY, Infante JR, Conry RM, Rabinowitz G et al (2021) Phase 1 trial of ALRN-6924, a dual inhibitor of MDMX and MDM2, in patients with solid tumors and lymphomas bearing wild-type TP53. *Clin Cancer Res* 27: 5236–5247
- Schmitt AM, Chang HY (2016) Long noncoding RNAs in cancer pathways. *Cancer Cell* 29: 452–463
- Schmitt AM, Garcia JT, Hung T, Flynn RA, Shen Y, Qu K, Payumo AY, Peres-da-Silva A, Broz DK, Baum R et al (2016) An inducible long noncoding RNA amplifies DNA damage signaling. *Nat Genet* 48: 1370–1376

- Sharma S, Findlay GM, Bandukwala HS, Oberdoerffer S, Baust B, Li Z, Schmidt V, Hogan PG, Sacks DB, Rao A (2011) Dephosphorylation of the nuclear factor of activated T cells (NFAT) transcription factor is regulated by an RNA-protein scaffold complex. *Proc Natl Acad Sci USA* 108: 11381–11386
- Shi D, Gu W (2012) Dual roles of MDM2 in the regulation of p53: ubiquitination dependent and ubiquitination independent mechanisms of MDM2 repression of p53 activity. *Genes Cancer* 3: 240–248
- Tong X, Liu S (2019) CPPred: coding potential prediction based on the global description of RNA sequence. *Nucleic Acids Res* 47: e43
- Vassilev LT (2007) MDM2 inhibitors for cancer therapy. *Trends Mol Med* 13: 23–31
- Volders PJ, Anckaert J, Verheggen K, Nuytens J, Martens L, Mestdagh P, Vandesompele J (2019) LNCipedia 5: towards a reference set of human long non-coding RNAs. *Nucleic Acids Res* 47: D135–D139
- Wade M, Wang YV, Wahl GM (2010) The p53 orchestra: Mdm2 and Mdmx set the tone. *Trends Cell Biol* 20: 299–309
- Wang S, Wang Y, Zhang Z, Zhu C, Wang C, Yu F, Zhao E (2021) Long non-coding RNA NRON promotes tumor proliferation by regulating ALKBH5 and Nanog in gastric cancer. *J Cancer* 12: 6861–6872
- Willingham AT, Orth AP, Batalov S, Peters EC, Wen BG, Aza-Blanc P, Hogenesch JB, Schultz PG (2005) A strategy for probing the function of noncoding RNAs finds a repressor of NFAT. *Science* 309: 1570–1573
- Xiong T, Huang C, Li J, Yu S, Chen F, Zhang Z, Zhuang C, Li Y, Zhuang C, Huang X et al (2020) LncRNA NRON promotes the proliferation, metastasis and EMT process in bladder cancer. *J Cancer* 11: 1751–1760
- Yao RW, Wang Y, Chen LL (2019) Cellular functions of long noncoding RNAs. *Nat Cell Biol* 21: 542–551
- Yao Z, Xiong Z, Li R, Liang H, Jia C, Deng M (2018) Long non-coding RNA NRON is downregulated in HCC and suppresses tumour cell proliferation and metastasis. *Biomed Pharmacother* 104: 102–109
- Yoeli-Lerner M, Yiu GK, Rabinovitz I, Erhardt P, Jauliac S, Toker A (2005) Akt blocks breast cancer cell motility and invasion through the transcription factor NFAT. *Mol Cell* 20: 539–550
- Yu F, Yao H, Zhu P, Zhang X, Pan Q, Gong C, Huang Y, Hu X, Su F, Lieberman J et al (2007) Let-7 regulates self renewal and tumorigenicity of breast cancer cells. *Cell* 131: 1109–1123
- Zuker M (2003) Mfold web server for nucleic acid folding and hybridization prediction. *Nucleic Acids Res* 31: 3406–3415